Iraqi Journal of Physics, 2026
https://doi.org/10.30723/ijp.v24i3.1350

Vol.24, No.3, PP.74-87
P-ISSN: 2070-4003
E-ISSN: 2664-5548

Characterization of Gliding Arc Plasma and Study of Its Grafting Effect on the Surface Properties of PVA and MMA

Mohammed A. Ismail[1*] and Saba J. Kadhem[1]
[1]*Department of Physics, College of Science, University of Baghdad, Baghdad, Iraq*
[*]Corresponding author: mohammed.i@sc.uobaghdad.edu.iq

Abstract

This study constructed a gliding arc plasma generation system operating at atmospheric pressure, using two stainless steel electrodes in an inverted V-shape powered by a high-voltage supply. Argon gas was introduced to generate plasma, and emission spectroscopy was used to analyze plasma parameters at varying gas flow rates. The results showed that higher gas flow rates increased electron temperature and electron density, indicating enhanced plasma ionization. In the second phase, methyl methacrylate (MMA) and polyvinyl alcohol (PVA) surfaces were modified via gliding arc plasma treatment for 5 min. to improve substrate adhesion. Post-treatment analysis was performed using Fourier transform infrared spectroscopy (FTIR) and field-emission scanning electron microscopy (FE-SEM). FE-SEM analysis revealed significant plasma-induced morphological changes, with PVA films developing nanoparticle chains and increased surface roughness at higher flow rates, whereas MMA films exhibited smoother and more homogeneous surfaces due to their hydrophobic nature. FTIR identified key vibrational bands (O-H, C-H, C=O, and C=C in PVA; C-H, C=O, and C-O in MMA), confirming chemical modification following plasma exposure. These findings highlight the potential of gliding arc plasma treatment for polymer surface modification in applications such as biomedical devices, coatings, textiles, and electronics.

Article Info.

Keywords:
Gliding Arc Discharge Plasma, Emission Spectra, Plasma Polymerization, Methyl Methacrylate (MMA), Polyvinyl Alcohol (PVA).

Article history:
Received: Jul.20, 2024
Revised: Jan. 27, 2025
Accepted:Feb.15, 2025
Published:Jun.01 2026

1. Introduction

Plasma is an ionized gas that consists of negative ions, atoms, and electrons [1, 2]. They are classified into thermal and non-thermal plasma [3]. Thermal plasma is characterized by high ionization levels [4]. It is associated with Joule heating and thermal ionization. This enables high-energy delivery at elevated operating pressures [5, 6]. The most important examples of thermal plasma sources include arc jets, plasma furnaces, plasma torches, tokamaks, and plasma spray systems [7, 8]. Non-thermal or cold plasma is characterized by electrons having a significantly higher temperature than the neutral ions and molecules present [9-11]. In this type of plasma, the particles do not reach thermal equilibrium, resulting in an uneven distribution of thermal energy [12,13]. Non-thermal plasma is notable for its capability to facilitate chemical reactions at comparatively low temperatures, in contrast to thermal plasma. This property makes non-thermal plasma particularly useful in processing polymers, including applications aimed at controlling their wettability. Emission spectra are a series of lines generated by analyzing (with a spectrometer) the light emitted from a substance as its atoms or molecules transfer from a higher energy state to a lower one [14, 15]. Plasma technology is considered one of the most important advanced methods for modifying surfaces and spreading polymer chains on substrates [16-18]. When monomers are exposed to plasma, they undergo polymerization and form covalent bonds with the activated surface, creating a polymer layer. Plasma polymerization is the synthesis of polymeric materials in the presence of plasma [19-21]. Plasma polymerization offers a variety of surface modifications, enabling changes to the surfaces of polymers and other materials. These advantages have contributed to the rapid advancement of plasma technology over the past few decades, leading to diverse

applications, such as enhancing adhesion in composite materials, creating protective coatings, fabricating membranes, and pursuing various medical applications, among others.

Plasma grafting polymerization (PRP) technology allows for precise control over surface chemistry and properties, enabling customized modification that enhances adhesion. This is particularly beneficial for improving the bonding of paints or other materials to surfaces that typically resist adhesion. Furthermore, plasma processing can enhance wettability, biocompatibility, and chemical resistance, resulting in more durable surfaces in harsh environments. It can also improve the mechanical properties of polymer films, including strength and flexibility [22-24]. PRP has numerous applications, including in biomedical devices, textiles, electronics, and advanced coatings. Its ability to modify surfaces without altering the properties of the base material makes it a versatile technology. Polymer grafting improves the morphology, chemical composition, and physical properties of the polymer. This method can enhance properties such as solubility, nanoscale shape, biocompatibility, and other attributes of the native polymer, thereby improving its overall performance, including charge transport. Polymer grafting is a process that involves linking monomers to the main polymer chain via covalent bonds, resulting in the formation of side chains. This grafting technique is valuable because it introduces a variety of functional properties into the polymer [25-29].

Polyvinyl alcohol (PVA) is a synthetic polymer known for its unique properties that make it suitable for numerous applications. Its importance stems from its biodegradability, making it environmentally friendly, and its water solubility. Furthermore, PVA is a non-toxic and safe material for medical and food applications [30, 31]. One of the most important applications of PVA is in the manufacture of industrial textiles and pharmaceutical packaging. Its non-toxic and biodegradable nature allows it to create a protective barrier that helps maintain the safety and efficacy of medicines. Additionally, when used in paper products, PVA enhances their strength, flexibility, and gloss. In the paint industry, PVA acts as a binder, improving paint adhesion to surfaces, increasing durability, and imparting a smooth finish [32]. Methyl methacrylate monomer (MMA) is a chemical compound widely used in various industries. Its importance is particularly evident in the plastic industry, where MMA is essential for the production of polymers such as polymethyl methacrylate (PMMA). Additionally, MMA plays a crucial role in dentistry, especially in the manufacture of dental fillings, and in the medical industry for the production of prosthetics and medical devices [33, 34].

This work focuses on generating and diagnosing gliding arc plasma through emission spectra analysis. The goal is to investigate the effect of the gas flow rate on plasma parameters. The generated plasma was also used to evaluate and modify polymer surfaces' chemical and morphological properties.

2. Experimental Work

Fig. 1 illustrates the system for generating gliding arc discharge plasma. It is composed of two stainless steel divergent, blade-shaped electrodes, each 1 mm thick and 2.5 cm in radius. These electrodes are mounted on a ceramic support, and the entire system is covered with a thin glass casing with two openings at the top for gas entry and at the bottom for the exit of the gas and plasma sparks. The gas employed was argon with different flow rates of 10, 15, 20, and 25 L/min. The electrodes were subjected to a high voltage of 10 kV with 100 mA, 50 Hz alternating current (AC). Reactive species were generated within the narrow plasma channel formed by the high voltage applied to the electrodes. A UV-NIR spectrometer (Thorlabs, model CCS100/M) was used to visually diagnose the plasma, which was connected to a computer that recorded the plasma emission spectra. The optical fibre was positioned parallel to the discharge electrodes and approximately 1 cm away. The plasma spectra were recorded for each flow rate.

Fig. 2 illustrates the application of the gliding arc plasma on the materials used, PVA and MMA. To prepare the solution, 0.5 g of PVA powder was mixed with 30 mL of non-ionic water. In contrast, the MMA was in a liquid form. A drop of the PVA polymer was applied

onto the surfaces of five thin slices, and gliding arc plasma was then directed onto these slices for five minutes at various argon gas flow rates (10, 15, 20, and 25 L/min). This process was repeated with the MMA monomer. The slides were positioned on a lab jack at a 3mm distance from the plasma torch to ensure that the plasma torch could adequately cover all areas of the material on the slides. The samples were analyzed using Fourier transform infrared spectroscopy (FTIR).

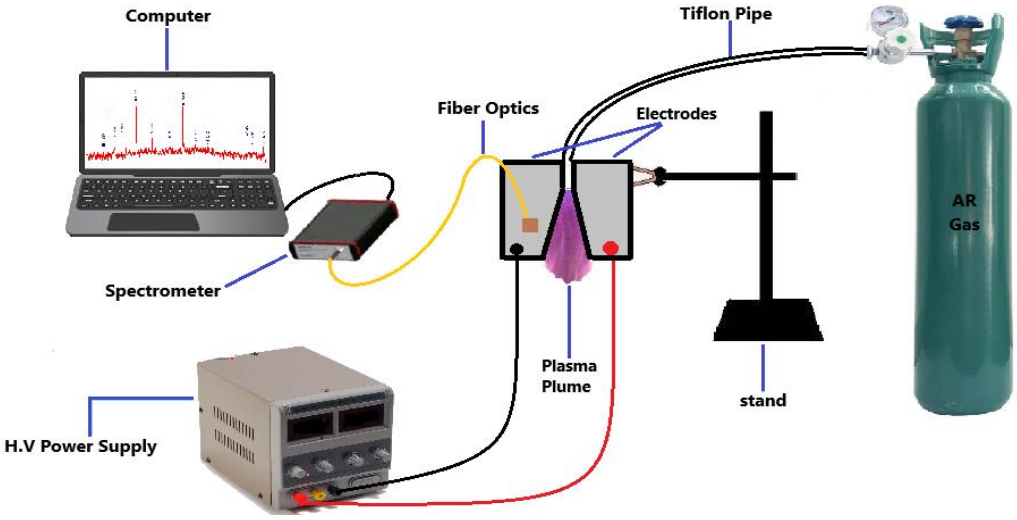

Figure 1: A Schematic diagram of the gliding arc plasma system.

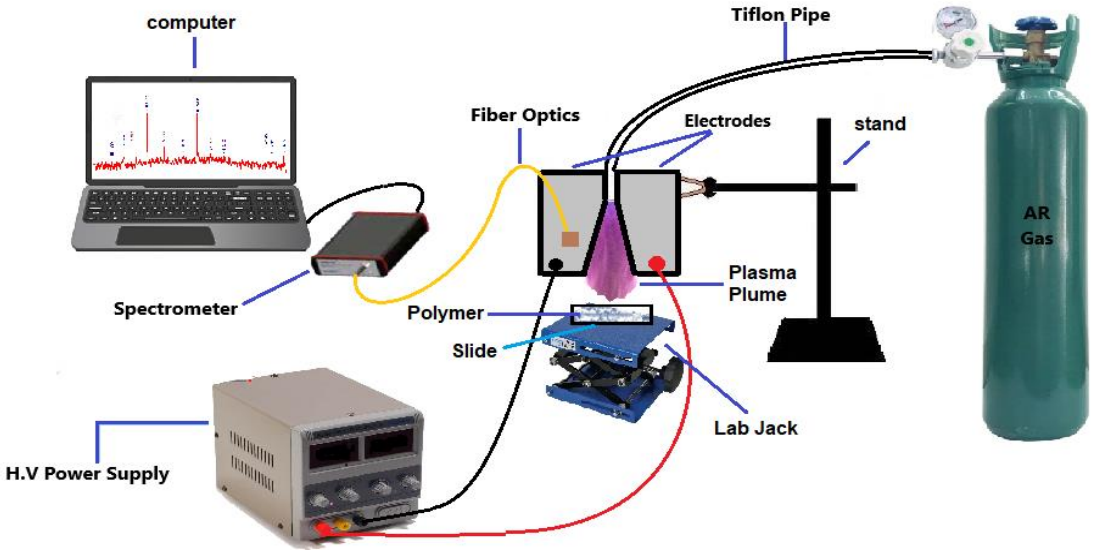

Figure 2: A Schematic diagram showing the projection of the gliding arc plasma onto the slide.

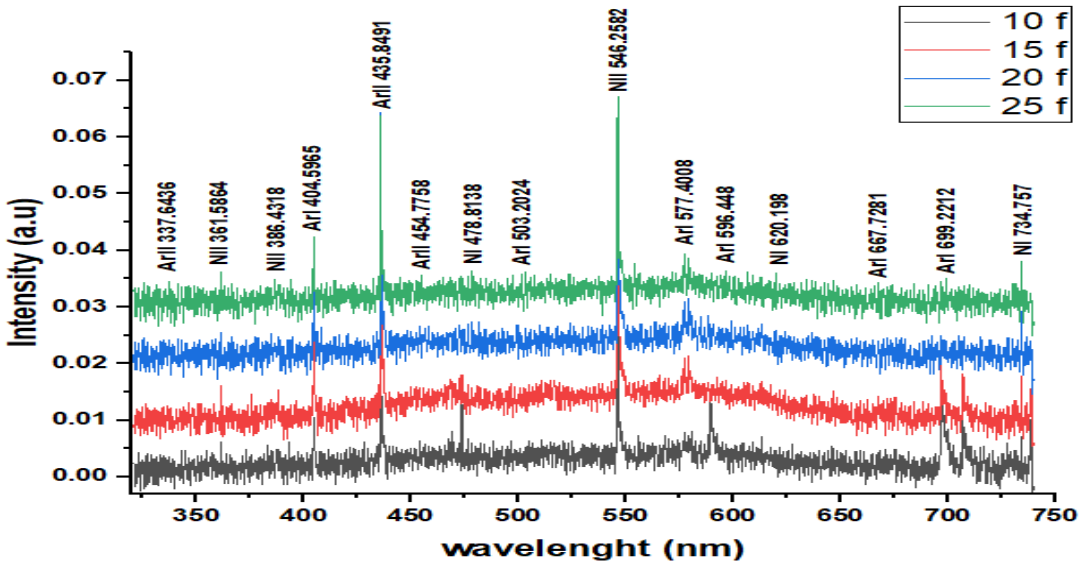

Figure 3: Emission spectra of the gliding arc plasma at different argon gas flow rates (10, 15, 20, and 25 L/min).

This technology relies on the interaction between infrared radiation and molecules. As infrared radiation passes through a sample, specific wavelengths are absorbed by the molecules, causing their chemical bonds to vibrate. The resulting spectrum, which displays absorption peaks at different wavelengths, was recorded. FTIR spectrometer (Shimadzu 1800, made in Japan) was utilized and covered a mid-infrared (mid-IR) wavelength range of 2.5 to 25 µm. This range was selected because it encompasses most vibrational movements of chemical compounds. The second analysis technique was field emission scanning electron microscopy (FE-SEM). FE-SEM is an analytical technique used to examine and study the surface of samples with high precision. It operates by directing a focused beam of electrons onto the sample. The interaction between the electrons and the sample generates various signals that provide information about the composition and surface characteristics. The FE-SEM used for this analysis was the MIRA III model from the Czech company Tescan. It is notable for its high accuracy, reaching down to nanometer levels, and its capability for 3D imaging of material surfaces.

3. Results and Discussion

Fig. 3 displays the emission spectra of the gliding arc plasma at different gas flow rates recorded with a UV-NIR spectrometer. The results align with data from the National Institute of Standards and Technology (NIST)[35]. The peaks were observed in the wavelength range of 310 to 750 nm. These peaks represent the wavelengths of the elements argon and nitrogen.

Variations in the peak intensity with the different argon gas flow rates are observed, highlighting the impact of gas flow rate on ionization and emission dynamics. The Boltzmann plot method was used to determine the electron temperature, and plasma density is expressed in Eq. (1):

$$\ln\left[\frac{\lambda_{j_i} I_{ji}}{hc\, A_{j_i g j}}\right] = -\frac{1}{KT}(E_j) + \ln\left|\frac{N}{U(T)}\right| \quad \textbf{(1)}$$

where I_{ji}, and g_j represent the relative emission line density between energy levels i and j, E_j is the excitation energy (in eV) for level I, A_{ji} is the probability of radiation transmission from level i to the lower level j, λ_{ji} is a wavelength (in nm), K is the Boltzmann constant, and N is a reference to the state's population densities.

Fig. 4 presents Boltzmann diagrams, which are used to analyze plasmas to determine their physical properties, such as electron temperature and energy distribution across various energy levels. The straight lines in these diagrams illustrate the relationships described by the Boltzmann equation (Eq. (1)). The slope of the line represents the plasma temperature; i.e., differences in the slopes of the diagrams indicate temperature variations. Additionally, R_2 is a statistical coefficient that measures the goodness of fit for the linear relationship and ranges from 0 to 1, with a value close to 1 indicating a strong linear correlation [36].

Fig. 5 presents the Voigt fitting profile of the emission spectra of the gliding arc plasma. The flexibility allows for thermal and collisional effecting any error coefficients. It was noted that the width of the peaks at FWHM increased with higher gas flow rates. This increase is attributed to the rising density of ionized particles, leading to a rise in temperature. Systems exposed to higher temperatures experience greater energy dispersion, resulting in the broadening of the peaks.

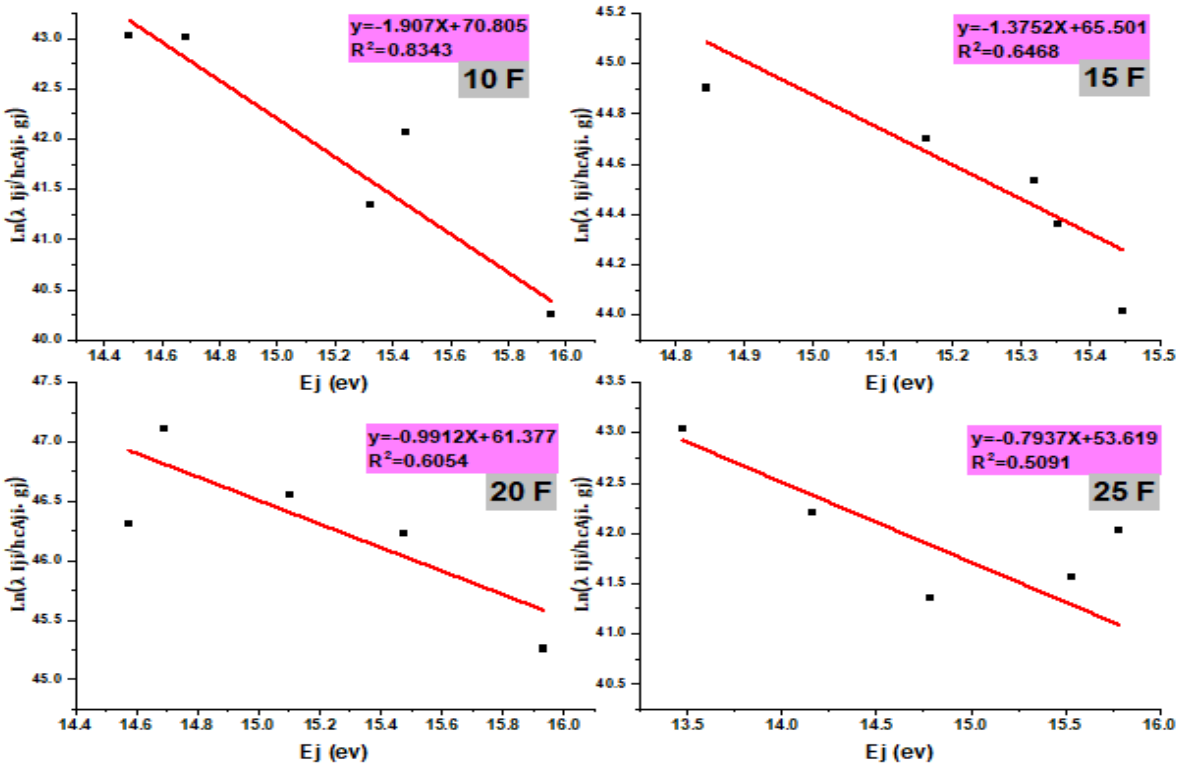

Figure 4: Boltzmann plots for the gliding arc plasma at different values of gas flow rates.

Fig. 6 shows the electron temperature (T_e) and density (n_e) as a function of the gas flow rates. It was noted that T_e increased from 0.52438 to 1.2599 eV, while the electron density increased from 8.2611 to 11.4723 × 10^{16} m^{-3}, as the gas flow rate was changed from 10 to 25 L/min, respectively. As the gas flow rate increases, the frequency of collisions between particles in the plasma also rises, resulting in a higher electron temperature. A greater gas flow rate leads to a higher ionized particle density, contributing to increased electron density. The rise in electron temperature and density is attributed to the energy absorption by the plasma particles.

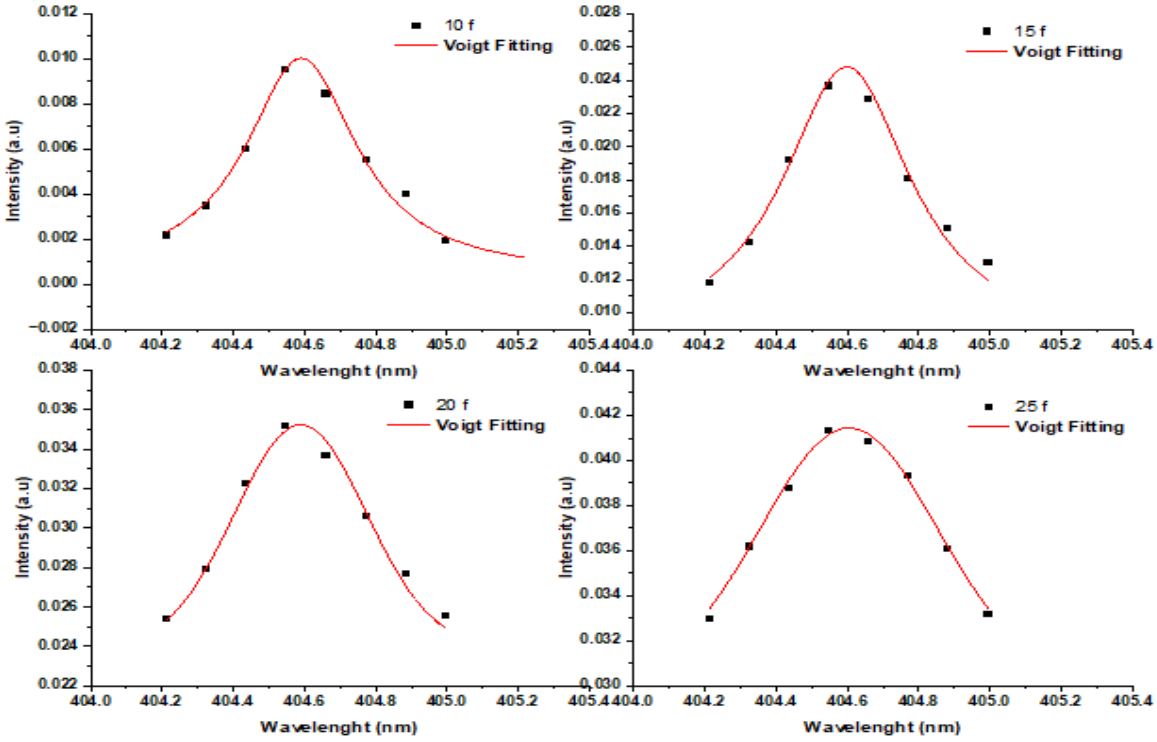

Figure 5: Voigt fitting profile of emission spectra of Ar I at (404.5965 nm).

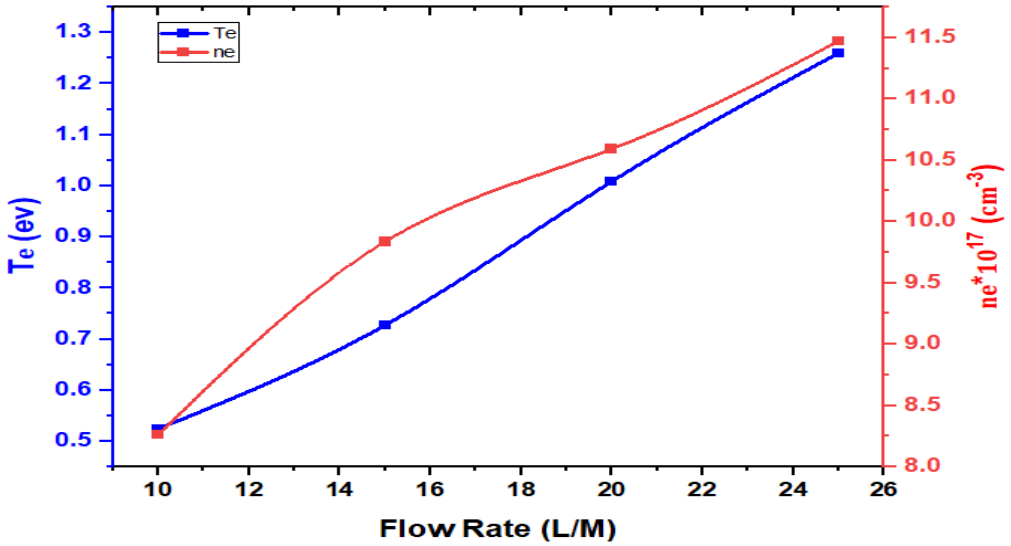

Figure 6: T_e and n_e as a function of argon gas flow rate.

Eq. (2) can be used to calculate Debye's length (λ_D), which defines the distance over which electrons can shield a charge within the plasma:

$$\lambda_D = \sqrt[2]{\frac{\varepsilon_O K_B T_E}{n_e e^2}} \quad \textbf{(2)}$$

The plasma frequency is expressed in Eq. (3):

$$w_{\rho e} = \sqrt{\frac{e^2 n_e}{\varepsilon_\circ m_e}} \quad \textbf{(3)}$$

where m_e is the electron mass; Eq. (4) gives the Debye Number (N_D):

$$N_D = \frac{4}{3}\pi\lambda_D^3 n_e \quad \textbf{(4)}$$

Table 1 presents the various parameters of the gliding arc plasma. These include the electron temperature (in eV), which indicates the average kinetic energy of electrons; n_e is the number density of electrons (in electrons per cubic meter); FWHM describes the width of the spectral peak (in nanometers), f_p is the plasma frequency of electrons (in Hertz), representing the vibrations of free electrons in the plasma.

Table 1: Gliding arc plasma parameters for the different argon gas flow rates.

F (L/min)	T_e (eV)	$n_e \times 10^{16}$ (m^{-3})	FWHM (nm)	$f_p \times 10^{12}$ (Hz)	$D \times 10^{-6}$ (cm)
10	0.52438	8.2611	4.956	2.5866	1.87207586
15	0.72716	9.8351	5.901	2.8224	2.02031319
20	1.00887	10.5933	6.356	2.92925	2.29293555
25	1.25992	11.4723	6.884	3.0485	2.46215742

Fig. 7 presents the FE-SEM images of the PVA films created by exposing a thin polymer layer to the gliding arc plasma generated at 2 and 4 L/min gas flow rates. The images demonstrate that the films have a smooth and homogeneous surface with chains of nanoparticles interspersed with small gaps and scattered clusters. A convergence in particle size is also evident, indicating that the surface is nearly uniform with some degree of roughness. This texture makes these membranes suitable for applications that require a large surface area.

It was noted that a decrease in the argon gas flow rate used to generate the gliding arc plasma resulted in more homogeneous films. The gliding arc plasma becomes more stable and less turbulent at low flow rates. This stability allows for a more uniform distribution of energy, which promotes the polymerization of monomers into long chains. Conversely, high flow rates can create turbulence and instability in the gliding arc plasma, leading to fluctuations in the energy delivered to the substrate. This can result in polymerization occurring in interrupted chains.

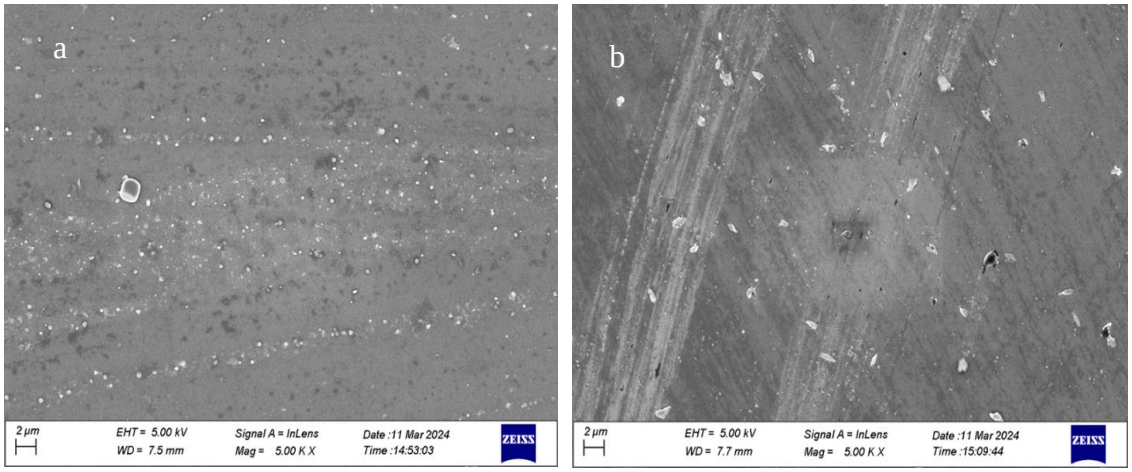

Figure 7: FE-SEM images of PVA for argon gas flow rates of (a) 2 L/min. (b) 4 L/min.

Fig. 8 displays the FE-SEM image of MMA films, which were converted into PMMA polymer through polymerization. This process was facilitated by plasma grafting using the gliding arc plasma method with argon gas flow rates of 2 and 4 L/min. The resulting PMMA

is a thermoplastic polymer known for its high transparency and excellent resistance to ultraviolet radiation and weather conditions. It is commonly referred to as acrylic glass or plexiglass. The images indicate that the PMMA films showed greater homogeneity compared to the PVA films. This difference can be attributed to the distinct compositions and chemical properties of the two polymers. PVA polymer contains hydroxyl groups (-OH), which make it hydrophilic and chemically reactive. In contrast, PMMA contains ester groups (-$COOCH_3$), which render it hydrophobic and less chemically reactive than PVA. PMMA films exhibit greater homogeneity due to their stable polymer structure and consistent interaction with plasma energy. Additionally, the hydrophobic nature of PMMA minimizes the impact of ambient humidity, resulting in more uniform films.

As the argon flow rate increased, the PVA and MMA surface characteristics changed. For PVA, at a flow rate of 2 L/min, the most notable feature is the regularity of the surface, with pore widths ranging from 50 to 100 nm. At a flow rate of 4 L/min, the effects of the plasma become more pronounced, resulting in increased roughness and wider pores, with widths reaching between 200 and 500 nm. For MMA, at a gas flow rate of 2 L/min, the effects were less pronounced compared to those of PVA. The surface structure was more stable, remaining smooth, with surface pores measuring approximately 30-70 nm. At a flow rate of 4 L/min, the surface pore size ranged from about 100-300 nm.

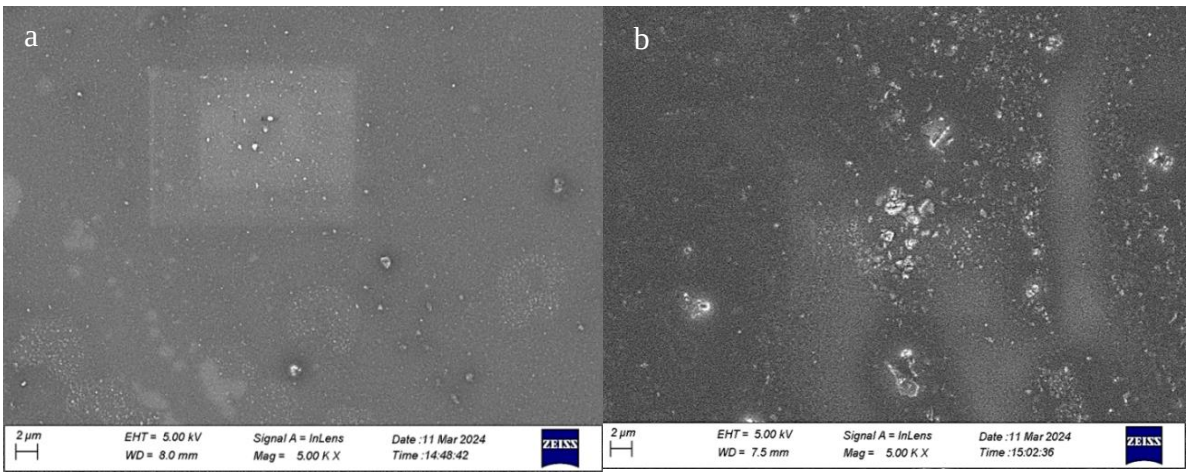

Figure 8: FE-SEM images of MMA for the argon gas flow are (a) 2 L/min and (b) 4 L/min.

Figs. 9-11 show the FTIR spectra of PVA for 1, 3, and 5 L/min gas flow rates. Each wavelength range corresponds to a specific type of molecular vibration. It was observed that the height and location of the peaks varied as the gas flow rate changed. This variation suggests the influence of the flow rate on the structural composition or the interaction of the material with the gaseous medium. The typical wavelengths associated with specific chemical bonds are as follows:

1- O-H stretching occurred at approximately 3300–3500 cm^{-1}. This band corresponds to the stretching vibration of the hydroxyl (OH) groups within the polymer backbone, typically characterized by asymmetric stretching vibrations.
2- C-H stretching was typically observed in the range of 2800-3000 cm^{-1}. This region corresponds to the stretching vibrations of carbon-hydrogen (C-H) bonds. Generally, C-H stretching vibrations are symmetrical due to the symmetrical distribution of carbon-hydrogen bonds around the carbon atom.
3- The stretching vibration of carbonyl groups (C=O) occurs around 1700–1750 cm^{-1}. This band corresponds to the asymmetric stretching of the C=O bond due to the differing

masses of carbon and oxygen atoms, which leads to unequal displacements during vibration.

4- The C-O stretching vibration occurred in the range of 1050–1300 cm^{-1}. This band corresponds to the vibration of carbon-oxygen C-O bonds. The varying weights of the carbon and oxygen atoms involved in the bond lead to asymmetry in both the C=O and C-O stretching vibrations.

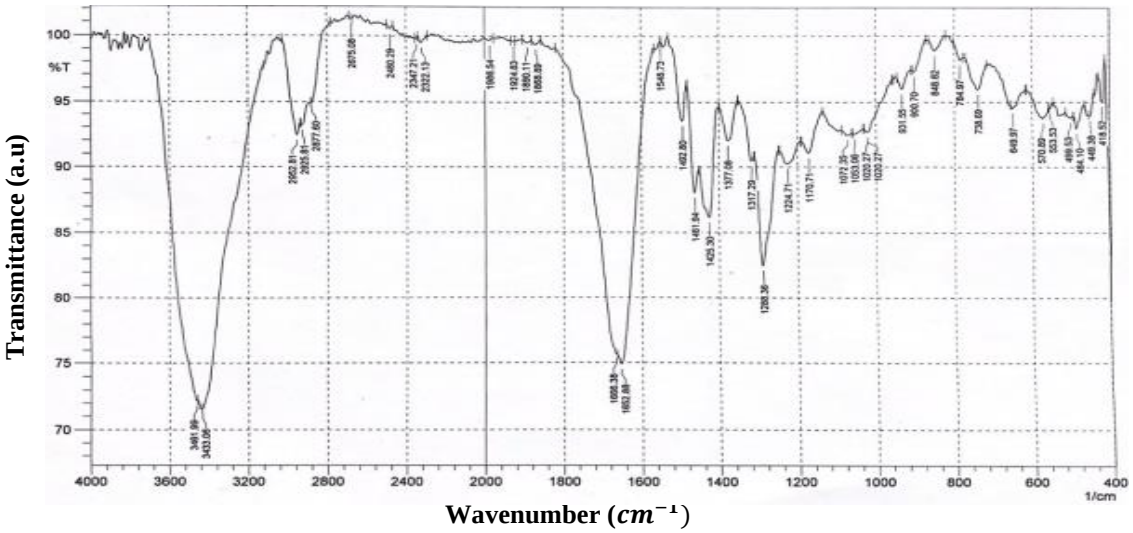

Figure 9: FTIR spectrum of PVA at a gas flow rate of 1 L/min.

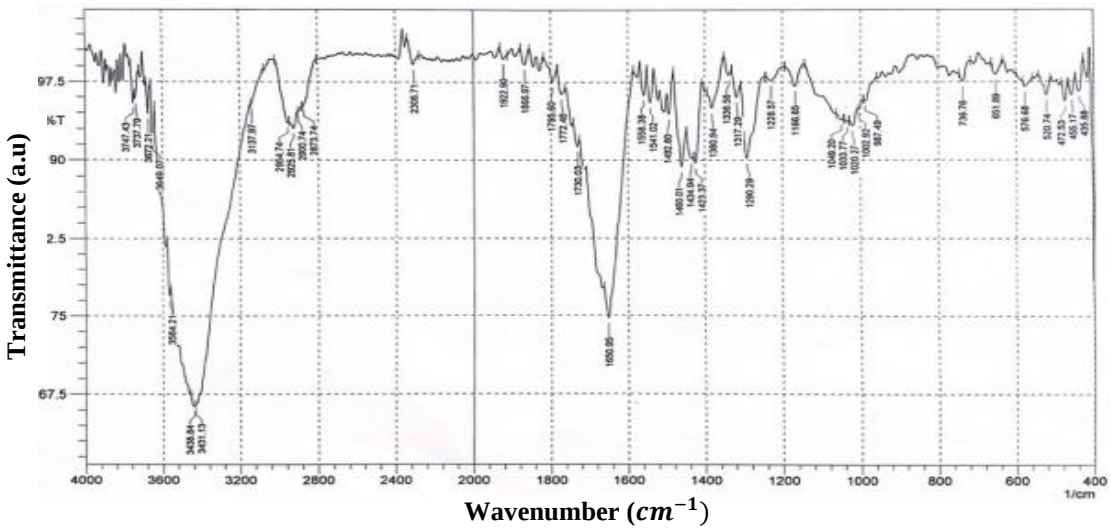

Figure 10: FTIR spectrum of PVA at a gas flow rate of 3 L/min.

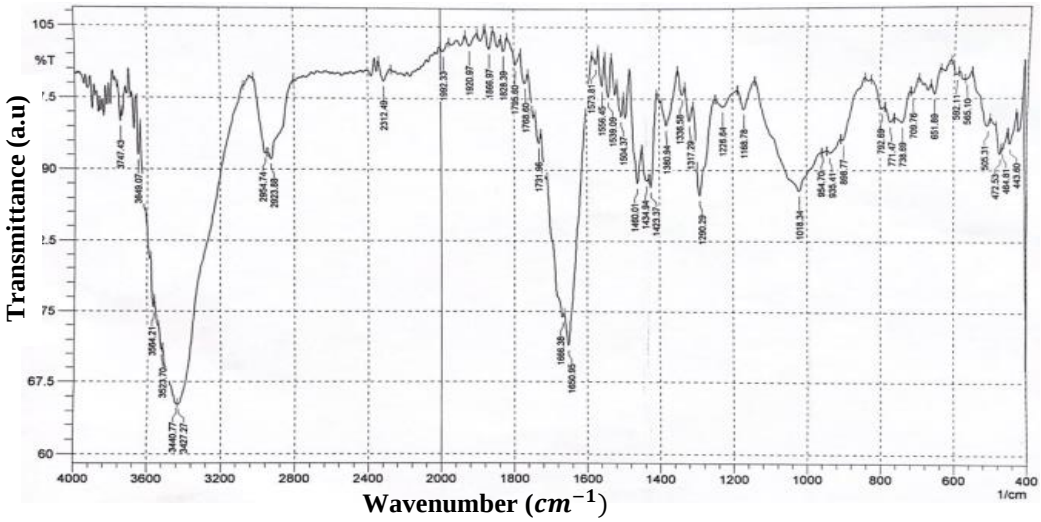

Figure 11: FTIR spectrum of PVA at a gas flow rate of 5 L/min.

Figs. 12-14 illustrate the FTIR examination of the MMA monomer, with typical wavelengths associated with specific chemical bonds:

1- C-H stretching was typically observed between 2800-3000 cm^{-1}. This band corresponds to the stretching vibration of the carbon-hydrogen (C–H) bonds found in the methyl groups of MMA. The C-H stretching vibration is usually symmetrical because the carbon-hydrogen bonds are evenly distributed around the carbon atom. Therefore, the C-H stretching vibration in MMA was generally symmetric.

2- The C=O stretching occurred in the range of 1720-1750 cm^{-1}. This band corresponds to the stretching vibration of the carbonyl group (C=O) within the ester functional group of methyl methacrylate (MMA). The C=O stretching vibration was asymmetric due to the different masses of the carbon and oxygen atoms, which caused unequal displacements during the vibration.

3- C=C Stretching at approximately 1630-1660 cm^{-1}. This band corresponds to the stretching vibration of the carbon-carbon double bond (C=C) found in the methacrylate group of MMA. The C=C stretching vibration was asymmetric, as it involves the stretching of the double bond between two different carbon atoms, resulting in unequal displacements during the vibration.

4- The range of 1100 to 1300 cm^{-1} corresponds to C-O stretching vibrations. This band represents the stretching of carbon-oxygen (C-O) bonds found in the ester functional group of MMA. Since the carbon and oxygen atoms involved in this bond have different masses, the C-O stretching vibration was asymmetrical, similar to the behavior seen in C=O stretching vibrations.

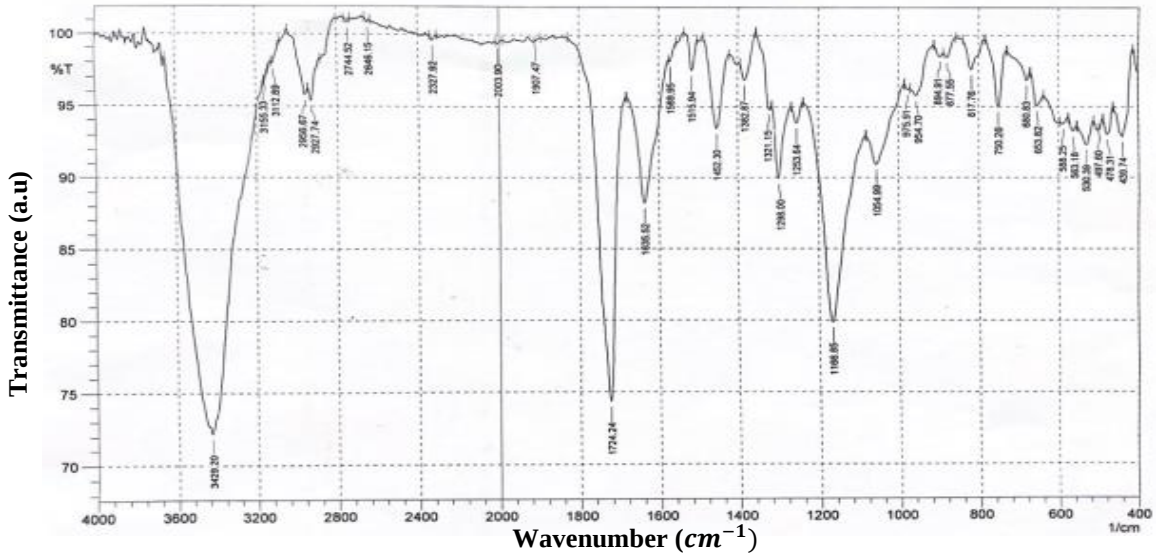

Figure 12: FTIR spectrum of PVA at a gas flow rate of 1 L/min.

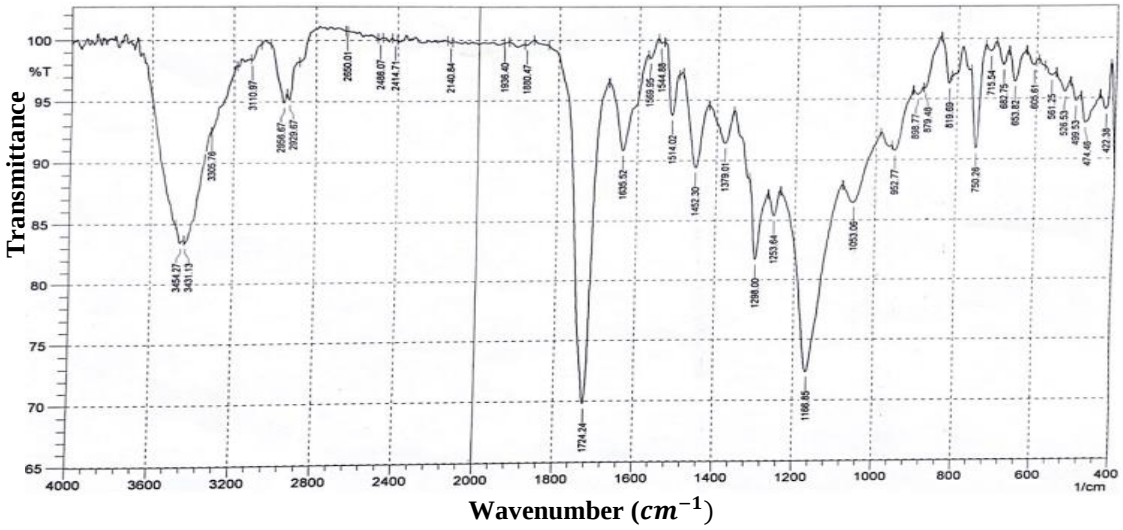

Figure 13: FTIR spectrum of PVA at a gas flow rate of 3 L/min.

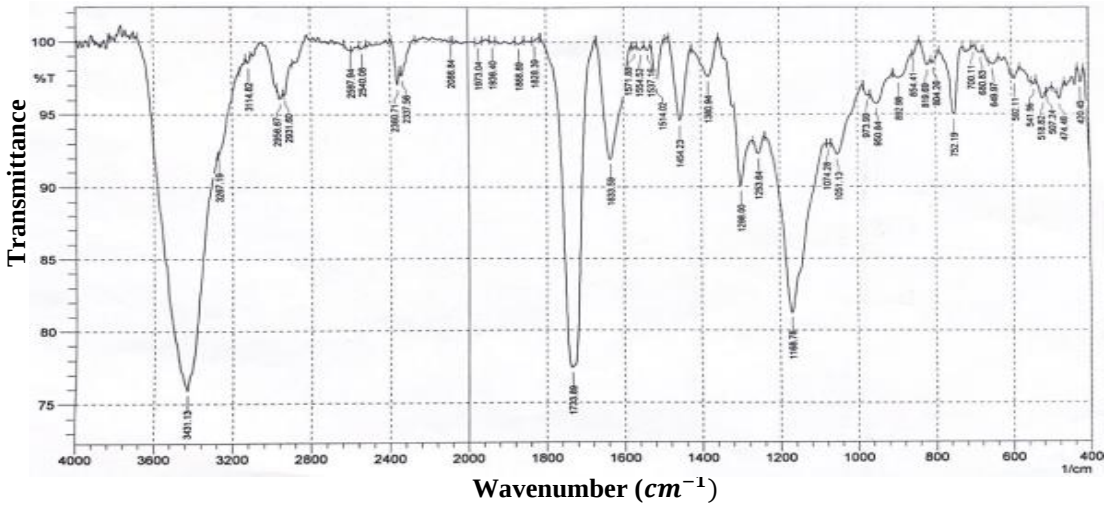

Figure 14: FTIR spectrum of PVA at a gas flow rate of 5 L/min.

4. Conclusions

Emission spectra analysis results showed that the Boltzmann diagram and Stark line amplitude analysis techniques provide measurements of both the electron temperature and the electron density in the plasma. It was demonstrated that increasing the gas flow rate leads to a higher collision rate between particles within the plasma, thereby enhancing the electron temperature. It was also observed that increasing the gas flow contributes to the rise in the density of ionized particles and thus an increase in the electron density. FE-SEM examination of PVA films revealed the formation of nanoparticle chains with gaps and agglomerations. In contrast, PMMA films had a more regular morphology due to their hydrophobic nature and stable polymer structure. These morphological differences suggest that these films could be employed in customized applications, depending on their surface properties. FTIR analysis of both PVA and PMMA also provided accurate information about the active chemical bonds. PVA spectra revealed distinct absorption bands for C-O, O-H, C-H, and C=O bonds, reflecting their molecular structures rich in hydroxyl and carbonyl groups. PMMA spectra exhibited absorption bands corresponding to methyl groups, C=C double bonds, and ester bonds, with distinct variations in asymmetric vibration within the C=C and C=O regions.

Conflict of Interest

The authors declare no conflicts of interest.

References

1. A. Bogaerts, E. Neyts, R. Gijbels, and J. Van der Mullen, Gas discharge plasmas and their applications, *Spectrochim. Acta. B At. Spectrosc.* **57**(4), 609 (2002). https://doi.org/10.1016/s0584-8547(01)00406-2.
2. S. A. Kadhim and H. R. Humud, Development of Low-Temperature Atmospheric Plasma Jet Sources for Biological Applications. *Iraqi J. Sci.* **64**(7), 4262 (2023). https://doi.org/10.24996/ijs.2023.64.7.18.
3. V. Nehra, A. Kumar, and H. K. Dwivedi, Atmospheric Non-Thermal Plasma Sources. *J. Eng.* **2**(1)**,** 53 (2008).
4. J. Heberlein, New approaches in thermal plasma technology. *Pure Appl. Chem.* **74**(3), 327 (2002). https://doi.org/10.1351/pac200274030327.
5. A. Fridman, A. Chirokov, and A. Gutsol, Non-thermal atmospheric pressure discharges. J. *Phys. D: Appl. Phys.* **38**(2), 2 (2005). https://doi.org/10.1088/0022-3727/38/2/r01.
6. F. A. Lazem and H. R. Humud, The thermal properties of gliding arc plasma produced by laboratory reverse vortex flow system. *Iraqi J. Phys.* **19**(50), 1 (2021). https://doi.org/10.30723/ijp.v19i50.680.
7. S. Ghorui, Unique Aspects of Thermal Plasma Torches and Reactor Design for Process Applications. *IEEE Trans. Plasma Sci.* **49**(2), 578 (2021). https://doi.org/10.1109/tps.2020.3006023.
8. S. Samal, Thermal plasma technology: The prospective future in material processing, *J. Clea. Prod.* **142**(4), 3131 (2017). https://doi.org/10.1016/j.jclepro.2016.10.154.
9. A. P. Harvey, I. A. Mohammed, U. Dahiru, and K. Zhang, Opportunities for process intensification using non-thermal plasmas, *Curr. Opin. Chem. Eng.* **41**, 100930 (2023). https://doi.org/10.1016/j.coche.2023.100930.
10. H. R. Humud, Strain specificity in antimicrobial activity of non-thermal plasma. *Iraqi J. Phys.* **11**, 110 (2019). https://doi.org/10.30723/ijp.v11i20.388.
11. A. Barjasteh, Z. Dehghani, P. Lamichhane, N. Kaushik, E. Ha Choi, and N. K. Kaushik, Recent progress in applications of non-thermal plasma for water purification, bio-sterilization, and decontamination, *Appl. Sci.* **11**(8), 3372 (2021). https://doi.org/10.3390/app11083372.
12. S. Busuioc, Quadrature-based lattice Boltzmann model for non-equilibrium dense gas flows, *Phys. Fluids.* **35**(1), 1 (2023). https://doi.org/10.1063/5.0135579.
13. N. A. Abdullah and S. J. Kadhem, Effect of Gas Flow Rate on Spectral Properties of Magnetically Stabilized Gliding Arc Discharge Plasma, *Iraqi J. Sci.* **65**(5), 2469 (2024). https://doi.org/10.24996/ijs.2024.65.5.11.
14. R. Zaplotnik, G. Primc, and A. Vesel, Optical emission spectroscopy as a diagnostic tool for characterization of atmospheric plasma jets, *Appl. Sci.* **11**(5), 2275 (2021). https://doi.org/10.3390/app11052275.
15. K. Aoyama, M. Kimura, H. Morohoshi, T. Takeda, M. Tanaka, and K. Yorita, Measurement of emission spectrum for gaseous argon electroluminescence in visible light region from 300 to 600 nm. Neutral Bremsstrahlung spectroscopy in Argon. *Nuclear Instruments and Methods in Physics Research Section A Accelerators Spectrometers Detectors and Associated Equipment*. **1025**, 166107 (2022). https://doi.org/10.1016/j.nima.2021.166107.

16. V. Luque-Agudo, M. Hierro-Oliva, A. M. Gallardo-Moreno, and M.L. González-Martín, Effect of plasma treatment on the surface properties of polylactic acid films, *Polym. Test.* **96**, 107097 (2021). https://doi.org/10.1016/j.polymertesting.2021.107097
17. A. Nikiforov, C. Ma, A. Choukourov, and F. Palumbo, Plasma technology in antimicrobial surface engineering. *J. Appl. Phys.* **131**, 1 (2022). https://doi.org/10.1063/5.0066724.
18. P. Sundriyal, M. Pandey, and S. Bhattacharya, Plasma-assisted surface alteration of industrial polymers for improved adhesive bonding, *Inter. J. Adhes. and Adhes.* **101**, 102626 (2020). https://doi.org/10.1016/j.ijadhadh.2020.102626.
19. J. C. de Oliveira, M. de M. Brioude, Airoudj, F. Bally-Le Gall, and V. Roucoules, Plasma polymerization in the design of new materials: looking through the lens of maleic anhydride plasma polymers, *Mater. Today Chem.* **23**, 100646 (2022). https://doi.org/10.1016/j.mtchem.2021.100646.
20. D. Hegemann, M. M. Hossain, E. Körner, and D. J. Balazs, Macroscopic Description of Plasma Polymerization Plasma Process. *Polym.* **4**(3), 229 (2007). https://doi.org/10.1002/ppap.200600169.
21. D. Thiry, S. Konstantinidis, J. Cornil, and R. Snyders, Plasma diagnostics for the low-pressure plasma polymerization process: A critical review, *Thin Solid Films.* **606**, 19 (2016). https://doi.org/10.1016/j.tsf.2016.02.058.
22. H. Zhang and Wei Li, Plasma-grafting polymerization on carbon fibers and its effect on their composite properties. *Appl. Surf. Sci.* **356**, 492 (2015). https://doi.org/10.1016/j.apsusc.2015.08.016.
23. J.C. de Oliveira, A. Airoudj, P. Kunemann, F. Bally-Le Gall, and V. Roucoules, Mechanical properties of plasma polymer films: a review, *SN Appl. Sci.* **3**, 6 (2021). https://doi.org/10.1007/s42452-021-04655-9.
24. G. Primc and M. Mozetič, Recent advances in corrosion inhibition of bonded NdFeB magnets, *Mater.* **17**(11), 2475 (2024). https://doi.org/10.3390/ma17112475.
25. P. Purohit, A. Bhatt, R. K. Mittal, M. H. Abdellattif, and T. A. Farghaly, Polymer Grafting and its chemical reactions, *Fron. Bioeng. Biotechnol.* **10,** 1 (2023). https://doi.org/10.3389/fbioe.2022.1044927.
26. M. D. Nothling, C. G. Bailey, L. Fallbrook, G. Wang, Y. Gao, D. R. McCamey, M. Monfared, S. M. Wong, J. E. Beves, and M. H. Stenzel, Polymer Grafting to Polydopamine Free Radicals for Universal Surface Functionalization, *J. Am. Chem. Soc.* **144** (15), 6992 (2022). https://doi.org/10.1021/jacs.2c02073.
27. R. Jayakumar, M. Prabaharan, R. L. Reis, and J. F. Mano, Graft copolymerized chitosan—present status and applications, *Carbohyd. Polym.* **62**(2), 142 (2005). https://doi.org/10.1016/j.carbpol.2005.07.017.
28. P. Eskandari, Z. Abousalman-Rezvani, H. Roghani-Mamaqani, M. Salami-Kalajahi, and H. Mardani, Polymer grafting on graphene layers by controlled radical polymerization, *Adv. Colloid Interface Sci.* **273**, 102021 (2019). https://doi.org/10.1016/j.cis.2019.102021.
29. O. Neděla, P. Slepička, and V. Švorčík, Surface modification of polymer substrates for biomedical applications. *Mater.* **10**(10), 1115 (2017). https://doi.org/10.3390/ma10101115.
30. L. Gautam, S. G. Warkar, S. I. Ahmad, R. Kant, and M. Jain, A review on carboxylic acid cross-linked polyvinyl alcohol: Properties and applications, *Polym. Eng. Sci.* **62**(2), 2 (2021). https://doi.org/10.1002/pen.25849.
31. A. Verma and M.A. Quraishi. Polyvinyl alcohol (PVA) as a biodegradable polymeric anticorrosive material: A review on present advancements and future directions, *Corros. Eng. Sci. Technol.* **57**(8), 796 (2022). https://doi.org/10.1080/1478422x.2022.2125621.
32. Z. W. Abdullah, Yu Dong, I. J. Davies, and S. Barbhuiya, PVA, PVA blends, and their nanocomposites for biodegradable packaging application. *Polym. Plast. Technol. Eng.* **56**(12), 1307 (2017). https://doi.org/10.1080/03602559.2016.1275684.
33. H. Kaur and Archana Thakur, Applications of poly(methyl methacrylate) polymer in dentistry: A review, *Mater. Today Proc.* **50**(5), 1619 (2021). https://doi.org/10.1016/j.matpr.2021.09.125.
34. M. J. D. Mahboub, Jean-Luc Dubois, F. Cavani, M. Rostamizadeh, and G. S. Patience, Catalysis for the synthesis of methacrylic acid and methyl methacrylate, *Chem. Soc. Rev.* **47**(20), 7703 (2018). https://doi.org/10.1039/c8cs00117k.
35. Z. M. Hasan and Q. A. Abbas, Influence of A.C. frequency on hollow magnetron sputtering discharge parameters. *Iraqi J. Phys.* **22**(1), 31 (2024). https://doi.org/10.30723/ijp.v22i1.1191.
36. C. Onyutha, A hydrological model skill score and revised R-squared, *Hydrol. Res.* **53**(1), 1 (2021). https://doi.org/10.2166/nh.2021.071.

تشخيص بلازما القوس المنزلق ودراسة تأثير تطعيمها على الخواص السطحية لبولي فاينيل الكحول ومثيل ميثا اكريليت

محمد عبدالرحمن اسماعيل[1] وصبا جواد كاظم[1]

[1]قسم الفيزياء، كلية العلوم، جامعة بغداد، بغداد، العراق

الخلاصة

صُممت في هذه الدراسة منظومة لتوليد البلازما باستخدام قوس انزلاقي تعمل عند الضغط الجوي، وذلك باستخدام قطبين كهربائيين من الفولاذ المقاوم للصدأ على شكل حرف V مقلوب، يتم تزويدهما بمصدر جهد عالٍ. استُخدم غاز الأرجون لتوليد البلازما، واستُخدمت مطيافية الانبعاث لتحليل خصائص البلازما عند معدلات تدفق غاز مختلفة. أظهرت النتائج أن ارتفاع معدلات تدفق الغاز يزيد من درجة حرارة الإلكترونات وكثافتها، مما يشير إلى تعزيز تأين البلازما. في المرحلة الثانية، عُدّلت أسطح ميثيل ميثاكريلات (MMA) وبولي فينيل الكحول (PVA) بمعالجة البلازما بالقوس الانزلاقي لمدة 5 دقائق لتحسين التصاق الركيزة. أُجري تحليل ما بعد المعالجة باستخدام مطيافية الأشعة تحت الحمراء بتحويل فورييه (FTIR) ومجهر المسح الإلكتروني ذي الانبعاث الميداني (FE-SEM). كشف تحليل FE-SEM عن تغيرات مورفولوجية ملحوظة ناتجة عن البلازما، حيث طورت أغشية PVA سلاسل من الجسيمات النانوية وزادت خشونة سطحها عند معدلات التدفق العالية، بينما أظهرت أغشية MMA أسطحًا أكثر نعومة وتجانسًا نظرًا لطبيعتها الكارهة للماء. كشفت تقنية FTIR عن نطاقات اهتزازية رئيسية (O-H، C-H، C=O، وC=C في بولي فينيل الكحول؛ C-H، C=O، وC-O في ميثيل ميثاكريلات)، مؤكدةً التعديل الكيميائي الذي أعقب التعرض للبلازما. تُبرز هذه النتائج إمكانات معالجة بلازما القوس المنزلق لتعديل أسطح البوليمرات في تطبيقات متنوعة كالأجهزة الطبية الحيوية، والطلاءات، والمنسوجات، والإلكترونيات.

الكلمات المفتاحيه: بلازما التفريغ القوسي، طيف الانبعاث الضوئي، بلمرة البلازما، ميثاكريلات الميثل، وكحول البولي فينيل.